

Kinetics of fly ash leaching in strongly alkaline solutions

Chen Chen · Weiliang Gong · Werner Lutze ·
Ian L. Pegg · Jianping Zhai

Received: 22 July 2010/Accepted: 8 October 2010/Published online: 26 October 2010
© Springer Science+Business Media, LLC 2010

Abstract We have leached fly ash samples from six power stations in potassium hydroxide solutions at a water-to-solid mass ratio of 40 g/g. A wet chemical method was developed which provides for a detailed characterization of the reactivity of fly ash. The leaching process could be divided into three stages. In stage one, reaction progress measured by the relative mass of fly ash reacted (α) was controlled by the rate of glass network dissolution while very little gel formed ($\alpha < 0.1$). In stage two, more gel (mainly oxides of Fe, Ca, Mg, and Ti) formed on the glass surface, and the rate of glass dissolution was limited by diffusion ($0.1 < \alpha < 0.45$). In stage three, zeolite crystallized on top of the gel layer, and an aluminosilicate gel formed in situ, while diffusion continued to control reaction progress ($\alpha > 0.45$). The data were modeled using a modified Jander equation and rate constants were calculated for each process. The rate constants for stage one reflect an intrinsic glass property, chemical durability, which increased linearly with increasing concentration of network formers in the glass phase of a fly ash.

Introduction

Efforts have been made to explore the processes involved in geopolymers product formation, as documented in several

reviews [1–5]. Only a few authors have studied the processes underlying fly ash reactivity in geopolymers systems [6–12]. In contrast, there is extensive literature in fly ash reactivity and reaction kinetics in fly ash/Portland cement systems. As an example, in fly ash/Portland cement systems fly ash reactivity is measured by the rate of reaction of fly ash with calcium hydroxide. Bumrongjaroen et al. [13] published a summary of methods measuring reactivity of fly ash in fly ash/Portland cement systems. Researchers used conductometric techniques to monitor the depletion of lime in solution as an indicator of reaction progress. The assumption is that Ca^{2+} dominates conductivity [14]. Other methods detect the amount of lime reacted by measuring the release of heat and changes of mass. For example, the lime concentration can be determined chemically by solvent extraction and by thermogravimetry and differential thermal analysis [15–18].

In a number of studies of geopolymers systems, reactivity of fly ash and other pozzolanic materials has been evaluated by measuring how much SiO_2 , Al_2O_3 , CaO , and other constituents have dissolved in alkaline solution at various water-to-solid ratios, i.e., 1–2000 g/g [9, 19–25]. Pietersen et al. [20] and Lee and van Deventer [22] conducted studies on the time dependence of dissolution of fly ash at different pH and temperatures. Published data quantify the mass of fly ash dissolved, while little was reported about precipitation and composition of gel and zeolite crystallization. No kinetic analysis has been reported.

The objective of this article is to contribute to the understanding of fly ash reactivity. We have developed a procedure to quantify reactivity of fly ashes in alkaline solutions. This procedure allows us to study fly ash dissolution and other processes individually at a higher water-to-solid ratio than used in geopolymers pastes. We discuss the significance of our findings for the process of

C. Chen · W. Gong (✉) · W. Lutze · I. L. Pegg
Vitreous State Laboratory, The Catholic University of America,
Washington, DC, USA
e-mail: gongw@vsl.cua.edu

C. Chen · J. Zhai
State Key Laboratory of Pollution Control and Resources
Reuse and School of the Environment, Nanjing University,
Nanjing 210093, People's Republic of China

geopolymerization. The relationship between the relative mass of fly ash reacted and the compressive strength of a geopolymers cement are presented in a separate article.

Materials and methods

Six type F fly ashes (low in calcium as defined in ASTM C618) were investigated. The compositions were analyzed by X-ray fluorescence spectroscopy (XRF) and the crystalline phases by X-ray diffraction (XRD). The loss on ignition (LOI) was measured following ASTM D7348-08. The mass fraction of glass was determined by difference. The chemical composition of the glass phase was calculated by subtracting LOI and the composition of the crystalline phases from the overall composition. The fraction of glass phase was also determined following the method by Fernández-Jiménez et al. [26], i.e., treatment of fly ash with dilute hydrofluoric acid to dissolve the glass. We have dried our fly ash samples at 105 °C instead of 1000 °C, as prescribed in [26]. Some of our fly ashes had fairly high contents of carbon, which upon heating to 1000 °C in air would burn off and obscure the measurement of the glass content. The mass fractions of the glass phase in the fly ashes range between 69 and 80 wt% after subtraction of LOI. Results are shown in Table 1. The mass fractions

determined indirectly by X-ray analysis agree very well with those measured by dissolution. The main constituents of the glass phase are SiO₂ and Al₂O₃.

Leaching experiments were conducted with 2.5 g fly ash in KOH solution. The molarities of the alkaline solutions were 1, 3, 5, 7.5, and 10 M, the reaction time was up to 14 days, temperatures were 20–75 °C. A water-to-fly-ash mass ratio of W/S = 40 was used in all the experiments. After leaching, the residue was filtered, washed, and then put in absolute ethanol to stop further hydration of the glass phase, then dried at 105 °C and weighed. The leachate was analyzed by direct current plasma atomic emission spectroscopy (DCP-AES). The dried fly ash residue was then immersed in diluted (1:20) HCl at room temperature for 3 h to dissolve reaction products on the glass surface. The residue was filtered, washed, dried at 105 °C, and weighed. Pristine fly ash samples treated with diluted HCl in this way yielded a background loss of ≈ 2 wt.

Measuring reactivity and reaction progress

Typically, the glass phase is the only reactive component of fly ash in an alkaline solution. Reactivity depends on glass composition and varies inversely with the chemical durability of the glass. Reactivity depends on the molarity

Table 1 Composition of the glass and crystal phases in pristine fly ash samples

Power plant Abbreviated Constituents	BSI BSI Weight percent	Wagner WAN BRS	Brandon shores BRS	Headwater HW	Newburgh NEW	Chalk point CHP
Glass						
Al ₂ O ₃	16.1	15.8	15.5	19.8	15.2	19.3
SiO ₂	46.3	43.5	44.3	43.9	41.6	43.8
Fe ₂ O ₃	3.4	4.4	2.8	4.2	5.0	9.4
CaO	1.0	1.1	1.0	1.4	3.3	1.0
MgO	0.7	0.7	0.6	0.9	0.9	0.8
BaO	<0.1	<0.1	<0.1	0.1	0.1	0.1
K ₂ O	2.5	2.4	2.2	2.6	2.2	2.5
Na ₂ O	<0.1	0.2	<0.1	0.4	0.5	<0.1
P ₂ O ₅	0.2	0.2	0.2	0.5	0.9	0.2
SO ₃	<0.1	0.8	0.5	1.2	1.3	0.9
SrO	0.1	0.1	<0.1	0.1	0.2	0.1
TiO ₂	1.9	1.8	2.1	1.5	1.4	1.6
Other ^a	0.2	0.3	0.2	0.4	0.4	0.3
Subtotal glass	72.4	71.2	69.5	77.0	72.8	80.0
LOI	12.6	10.3	13.7	9.6	5.4	3.3
Quartz	2.8	5.3	3.4	2.4	2.0	4.6
Mullite	12.2	13.2	13.4	7.3	13.4	8.8
Magnetite	<0.1	<0.1	<0.1	3.7	6.4	3.3
Total	100.0	100.0	100.0	100.0	100.0	100.0
Particle size >45 µm (%)	30.6	37	32.8	26.8	18.2	77.7

^a Comprises oxides of As, Cr, Cu, Ga, Mn, Ni, Zn, Zr, and rare-earth elements

and kind of alkali (Li, Na, and K), on the water-to-solid-ratio (W/S), temperature, and particle size. We apply “reactivity” to fly ash in its entirety, not only to the glass phase. Therefore, the reaction progress does not reach 100% in the presence of less reactive constituents.

Herein, we define reactivity by

$$\frac{d\alpha}{dt} = \frac{1}{m_0} \cdot \frac{dm_t}{dt} \quad (1)$$

and reaction progress by

$$\alpha_t = \frac{\Delta m(t)}{m_0} = \frac{m_0 - m_t}{m_0}, \quad (2)$$

where m_0 is the initial mass of fly ash and m_t is the residual mass at time t after leaching in alkali hydroxide and subsequent dissolution of reaction products with diluted HCl. In this study we measure increments of mass loss and characterize reactivity in terms of reaction progress. We measured α_t in two ways: directly by mass loss and indirectly by solution analysis. If m_0 is the mass of fly ash initially and m'_t is the residual mass after leaching in alkali hydroxide solution, then the apparent relative mass loss α'_t of the fly ash is

$$\alpha'_t = \frac{m_0 - m'_t}{m_0}. \quad (3)$$

If the molarity of the alkali and the W/S ratio are constant, then m'_t is only a function of temperature. Bearing in mind that frequently a surface layer (gel) forms on the glass surface, the leached fly ash samples were treated with hydrochloric acid to dissolve the gel, which was counted as reacted glass. The mass dissolved in acid originates from reacted but undissolved glass, and potentially from additional material, such as water, hydroxyl groups, and alkali ions. Hence, if α'_t in Eq. 3 is determined by a mass loss measurement, m'_t must be corrected for the additional material, δ_t , in the gel:

$$\alpha'_{t \text{ corr}} = \frac{m_0 - m'_t + \delta_t}{m_0} = \alpha'_t + \frac{\delta_t}{m_0}. \quad (4)$$

The mass fraction $\alpha'_{t \text{ corr}}$ can be measured directly by analyzing the alkaline leachate for all glass constituents and recalculating them as oxides, provided the glass does not contain a significant amount of the alkali metal of the leachant. If $\delta_t/m_0 \ll \alpha'_t$, we obtain $\alpha'_{t \text{ corr}} \approx \alpha'_t$, i.e., there should not be a significant difference between the results from solution analyses and mass loss measurements.

At higher reaction progress, crystals may form within or on top of the gel layer. We treat such phases also as part of the reacted glass because they may contain constituents, which otherwise would not be accounted for. However, if the crystals contain additionally constituents from the leachant, i.e., the alkali ion, hydroxyl groups, and/or water,

this treatment may introduce an error. Let the relative mass of gel and/or new crystals be β'_t :

$$\beta'_t = \frac{m'_t - m_t}{m_0}. \quad (5)$$

Here, m_t is the mass after dissolution of all surface precipitates in HCl. If β'_t is determined by mass loss measurement, the correction δ_t (Eq. 4) must be applied to obtain the fraction of fly ash converted into gel and crystals:

$$\beta'_{t \text{ corr}} = \frac{m'_t - m_t - \delta_t}{m_0} = \beta'_t - \frac{\delta_t}{m_0}. \quad (6)$$

Like $\alpha'_{t \text{ corr}}$, the mass fraction $\beta'_{t \text{ corr}}$ can be measured directly by analyzing the solution for all constituents of the dissolved gel and crystals and recalculating them as oxides.

If $\delta_t/m_0 \ll \beta'_t$, we obtain $\beta'_{t \text{ corr}} \approx \beta'_t$, i.e., there should not be a significant difference between the results from solution analyses and mass loss measurements. Finally, the overall reaction progress α_t is given by:

$$\alpha_t = \alpha'_{t \text{ corr}} + \beta'_{t \text{ corr}} = \frac{m_0 - m_t}{m_0}. \quad (7)$$

Equation 7 shows that the reaction progress of a fly ash can either be determined by solution analyses or by measuring the residual mass after exposure of the leached fly ash to HCl.

Results

Figure 1 shows the result of mass loss measurements on HW fly ash (7.5 M KOH, 40 °C). The two uppermost

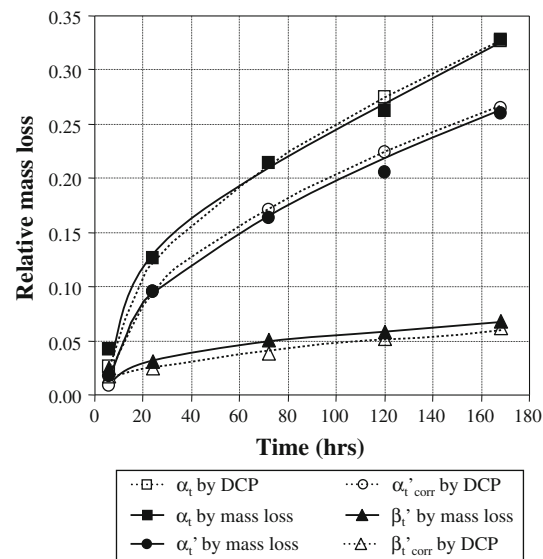


Fig. 1 Relative mass loss of HW fly ash in 7.5 M KOH at 40 °C

curves show reaction progress (Eq. 7), determined either by mass loss measurement (solid line) or calculated based on solution analyses (dotted line). The agreement of the results is within the limits of the experimental errors. The solid curve in the middle of the figure shows the relative mass loss α'_t (Eq. 3). The dotted curve shows $\alpha'_{t,\text{corr}}$ (Eq. 4), which was calculated based on leachate analyses. Values of $\alpha'_{t,\text{corr}}$ are slightly higher than respective values of α'_t because they include the correction δ_t (Eq. 4). The relative mass loss β'_t (Eq. 5) is shown on the bottom (solid curve). β'_t was determined by measuring masses of fly ash samples after dissolving the gel on the glass surface. The dotted curve shows the respective relative mass loss $\beta'_{t,\text{corr}}$ (Eq. 6), based on chemical analyses of the acid leachate. Equations 5 and 6 suggest that the dotted curve on the bottom of Fig. 1 runs below the respective solid curve, whereas Eqs. 3 and 4 suggest that the dotted curve $\alpha'_{t,\text{corr}}$ runs above the respective solid curve. This is in agreement with the experimental findings.

Figure 2a shows the effect of temperature on reaction progress in 7.5 M KOH. This temperature dependence is typical of all six fly ashes. At 60 and 75 °C reaction progress reaches its highest possible value after 2 weeks. Figure 2b shows the reaction progress at different KOH molarities at 75 °C. Reaction progress increases with increasing OH⁻ molarity. Except in 1 M KOH solution, α approaches values of 0.7–0.8, which correspond to the mass fractions of glass in HW fly ash (Table 1). At $\alpha_t > 0.45$, $M_{\text{KOH}} > 3$, and $T \geq 35$ °C, an additional phase, Linde F zeolite ($\text{KAISiO}_4 \cdot 1.5\text{H}_2\text{O}$) appeared.

Figure 3 shows X-ray diffraction patterns of HW fly ash leached in 7.5 M KOH solution at 50 °C. Mullite and quartz are phases present in the pristine fly ash ($\alpha = 0$). All fly ash patterns in Fig. 6 show a halo between $20^\circ < 2\theta < 35^\circ$, indicating the presence of amorphous material, i.e., glass in the pristine fly ash and glass and gel in leached samples. As the reaction progress increases from zero to 0.66, an

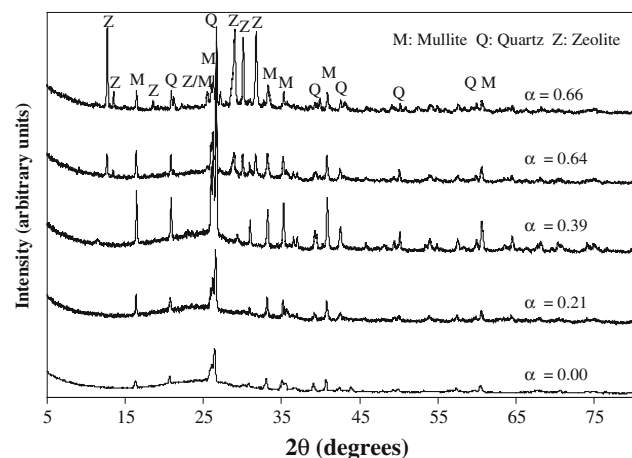


Fig. 3 Headwater fly ash, evolution of crystalline phases as a function of reaction progress

additional crystalline phase (marked Z) appears. This phase was identified as Linde F zeolite ($\text{KAISiO}_4 \cdot 1.5\text{H}_2\text{O}$, JCPDS 38-0216). The yield of zeolite increased strongly with increasing reaction progress (compare $\alpha = 0.64$ and 0.66 in Fig. 3). The pattern for $\alpha = 0.39$ was measured with increased sensitivity compared with the other patterns. There was no evidence of zeolite yet. A more detailed XRD study with all fly ashes at different leaching conditions showed that: (a) Linde F zeolite was the only new phase, (b) Linde F zeolite was observed at temperatures as low as 35 °C and $\alpha > 0.45$, and (c) the KOH concentration had to be > 3 M for the zeolite to crystallize. Linde F zeolite was not observed at 20 °C because the highest reaction progress was 0.14 in 7.5 M KOH, far less than 0.45. The reaction rate at 20 °C was very small.

Figure 4 shows a secondary electron image of leached HW fly ash. Glass particles are covered with crystals. Inlay (a) shows the morphology of Linde F zeolite crystals [27]. Inlay (b) shows the microstructure of partially leached glass particles (backscattered electron image). Between a

Fig. 2 Reaction progress of HW fly ash; **a** as a function of temperature in 7.5 M KOH, **b** as a function of KOH molarity at 75 °C

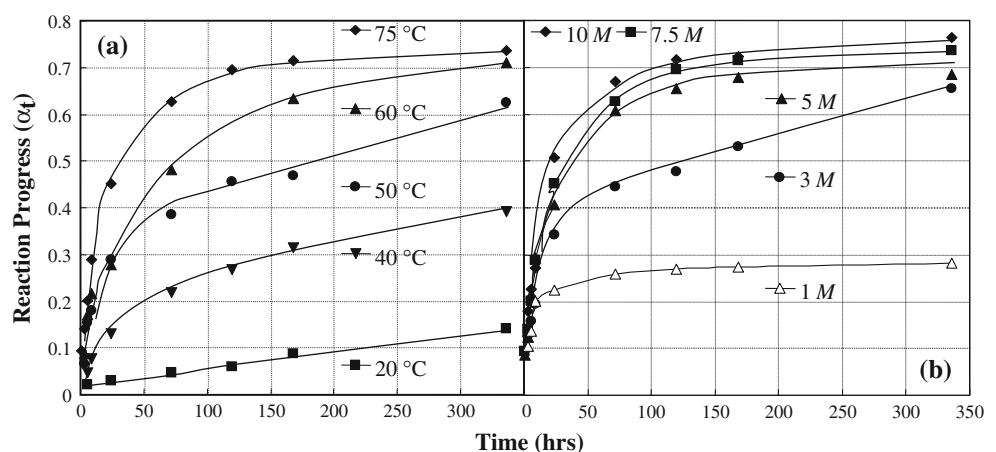
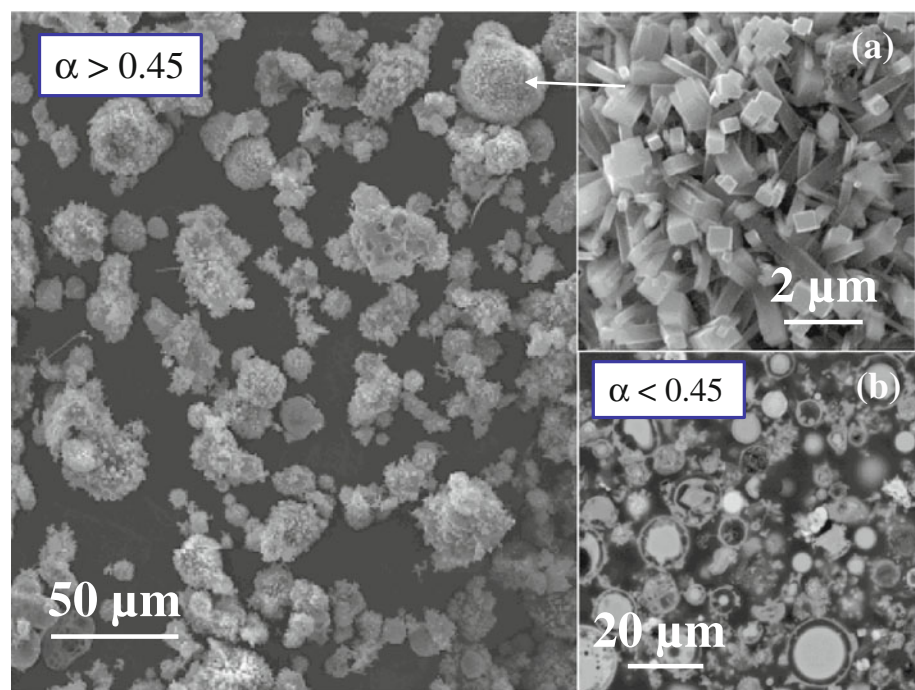


Fig. 4 SEM micrograph of HW fly ash particles after leaching in 7.5 M KOH solution at 75 °C and 3 days ($\alpha = 0.62$); *inlay* **a** Linde F zeolite crystals, **b** gel layers on glass



bright thin layer and the unreacted core is a darker gel phase, which contains more SiO₂ and Al₂O₃ and much less Fe₂O₃ than the outer layer.

Figure 5a shows the partitioning of SiO₂ and Al₂O₃ between the aqueous phase and the gel after leaching HW fly ash in 7.5 M KOH at 40 °C. We show the partitioning by plotting relative masses of oxides (g/g-fly ash) versus reaction progress. Since practically no other glass constituents were found in the leachate, the sum of SiO₂ and Al₂O₃ is the total mass of glass dissolved (open circles). The mass of SiO₂ and Al₂O₃ found in the gel layer is relatively small but does not add up to the total mass of gel (filled circles). Analysis of the dissolved gels showed that Fe₂O₃, and to a lesser extent CaO, MgO, and TiO₂, make up the difference. The overall finding of our analyses is that 80% of the reacted glass is dissolved and about 20% forms gel, up to $\alpha_t = 0.33$.

Fig. 5 Relative masses of major oxides in the leachate and in the gel as functions of reaction progress (α) in 7.5 M KOH; **a** at 40 °C, **b** at 75 °C

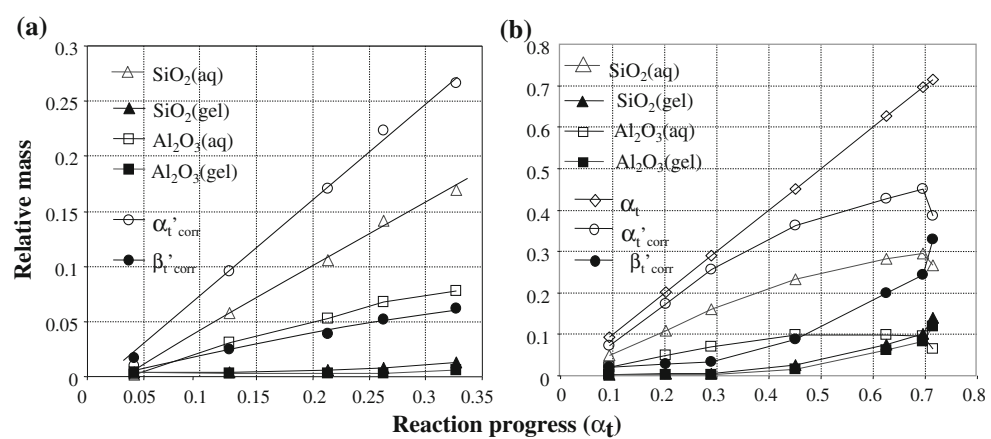


Figure 5b shows mass fractions (g/g-fly ash) of SiO₂ (open triangles) and Al₂O₃ (open squares) in 7.5 M KOH at 75 °C. Summation of SiO₂ and Al₂O₃ yielded $\alpha'_{t \text{ corr}}$, (Eq. 4), the relative mass loss of the fly ash after leaching. Figure 5b also shows relative masses of SiO₂ (solid triangles) and Al₂O₃ (solid squares) in the gel. Summing these oxides together with other glass constituents (Fe₂O₃, CaO, MgO, TiO₂—not shown) yields $\beta'_{t \text{ corr}}$, (Eq. 6), the relative mass of reacted glass retained as gel. Summation of $\alpha'_{t \text{ corr}}$ and $\beta'_{t \text{ corr}}$ yields α : the total reaction progress (Eq. 7). The behavior of the major oxides was the same at 40 and 75 °C as long as α_t was <0.33. The contribution of gel to the total reaction progress increased to almost 50% at higher α_t values, reaching 0.34 g/g-fly ash ($\beta'_{t \text{ corr}}$) compared with 0.38 g/g-fly ash dissolved ($\alpha'_{t \text{ corr}}$) at $\alpha_t \approx 0.71$. In comparison, the relative mass of gel β'_{t} (Eq. 5) determined by mass loss measurement was 0.654 g/g-fly ash at $\alpha_t \approx 0.71$.

Thus, the δ_t value in Eqs. 4 and 6 was 0.316 g/g-fly ash, showing that δ_t is not negligible at $\alpha_t > 0.33$ (see “Discussion”).

Discussion

Khawam and Flanagan [28] published a review of processes, models, and rate laws governing solid-state reactions. After testing various models, we adopted a rate equation first published by Jander [29]:

$$[1 - (1 - \alpha)^{1/3}] = K_2 \cdot t, \quad (8)$$

where $K_2 = k_2/r^2$ and k_2 has the dimensions of a diffusion coefficient, i.e., K_2 is a time constant; r is the radius of a sphere, t is time and α is reaction progress. This rate equation applies to a solid/liquid system if the reaction takes place beneath a surface layer and the rate is controlled by diffusion of species toward or away from the reaction front.

Kondo et al. [30] have modified the Jander equation for broader application by introducing the reaction grade N :

$$[1 - (1 - \alpha)^{1/3}]^N = K_N \cdot t \quad (9)$$

or in linear form:

$$\ln[1 - (1 - \alpha)^{1/3}] = \frac{1}{N} \ln K_N + \frac{1}{N} \ln t. \quad (10)$$

Equation 10 can be used to model consecutive and sometimes overlapping processes. Following Kondo et al. [30], N has the following meaning:

- (1) $N \leq 1$: The process is controlled by a chemical reaction at the surface or by dissolution of reactants or precipitation of reaction products. This is the “geometrical contracting sphere/cube model” derived by Khawam and Flanagan [28].

- (2) $1 < N \leq 2$: The process is controlled by diffusion of reactants through a porous layer of reaction products. This is the diffusion model derived by Khawam and Flanagan [28].
- (3) $N > 2$: The process is controlled by diffusion of reactants through a dense layer of reaction products.

Shi and Day [38] used Eq. 9 to model reactions of an activator (Na_2SO_4 and CaCl_2) in a lime-pozzolan blend. Dabic et al. [31] and Krstulovic and Dabic [32] modeled cement hydration. Cabrera and Rojas [33] modeled hydration of the metakolin-lime-water system.

Figure 6a shows plots of Eq. 10 fitted to reaction progress data for HW fly ash (7.5 M KOH, various temperatures). The slopes of the straight lines are the inverse of the reaction grade N . At 20 °C only one curve with a slope of $1/N = 1$ was obtained for data up to 14 days (filled squares). At 40 °C, the data are best represented by two curves. At low reaction progress the slope is $1/N = 1$, at higher reaction progress it is $1/2$, i.e., $N = 2$. At 50 °C a second change in slope, i.e., a third reaction grade $N > 2$ is indicated. At 60 and 75 °C, $N = 1$ is no longer seen.

Figure 6b shows reactivities for six fly ashes. Four fly ashes are practically indistinguishable in terms of reactivity. NEW fly ash shows a slightly higher and CHP a lower reactivity. For CHP the mechanism with $N > 2$ is absent. In NEW the glass particles are smaller and in CHP larger than in the other fly ashes (Table 1). This explains the deviation from the other curves.

It is likely that the glass dissolution mechanism ($N = 1$) is the same as that proposed for borosilicate nuclear waste glasses in aqueous solutions, i.e., breaking of Si–O–Si and/or Si–O–Al bonds and release of $\text{Si}(\text{OH})_4^-$ and $\text{Al}(\text{OH})_4^-$ species, where the rate-limiting step could be the detachment of an –O–Si(OH)₃ group [34]. Several authors have shown that $(\text{SiO}(\text{OH})_3)^-$ is the dominant species in solution at around pH = 11 and that the concentration of

Fig. 6 Analysis of reaction kinetics of HW fly ash leached in 7.5 M KOH; **a** at different temperatures, **b** six fly ashes at 75 °C

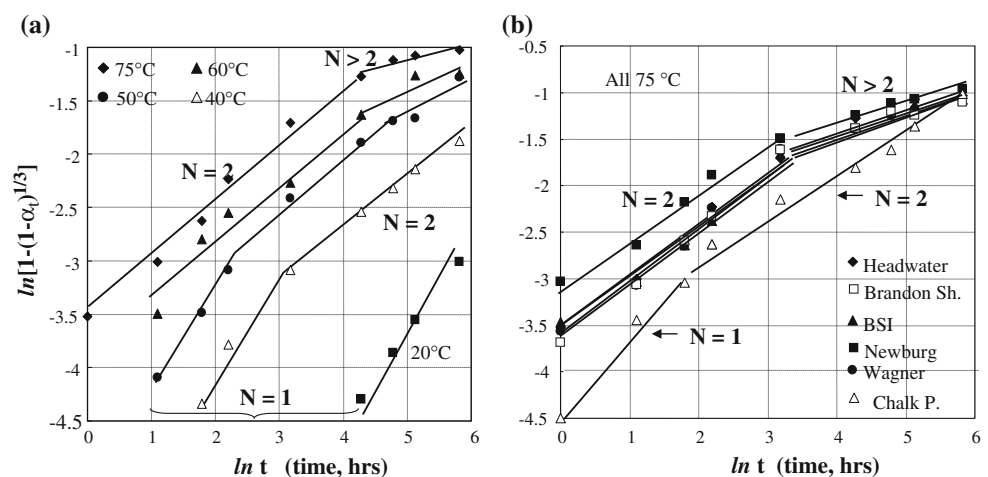
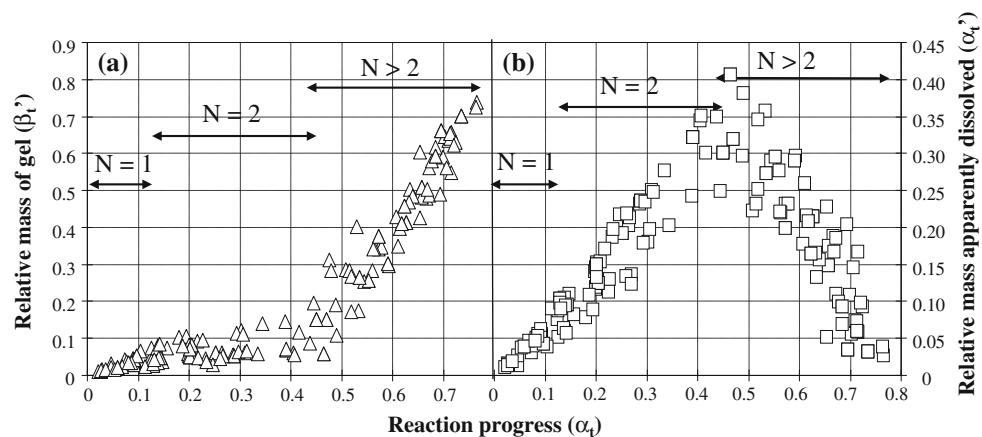


Fig. 7 Relative mass of gel produced (β'_t) and fly ash dissolved (α'_t) as a function of reaction progress (α_t); data for six fly ashes, all temperatures, and all KOH ≥ 5 M



($\text{SiO}_2(\text{OH})_2^{2-}$ increases with increasing pH [35, 36]. Silicon and aluminum hydroxy complexes are the starting species for geopolymers [37–40].

Next we relate the reaction grades N to what happens at the surface of the glass with increasing reaction progress. Figure 7a shows the relative mass of gel (β'_t) and Fig. 7b shows the relative mass of glass apparently dissolved (α'_t , Eq. 1) as a function of reaction progress. We identify three stages in Fig. 7, and relate them to reaction grades. When α_t is small, the gel layer is thin (0.1 μm) and does not constitute a transport barrier. Glass network dissolution is rate limiting ($N = 1$). With increasing reaction progress more gel is generated. The thin layer remains in place, while a Si–Al-rich gel forms beneath (Fig. 4, inlay b). For glass to dissolve, OH^- and H_2O must be transported to the surface. Evidently, diffusion controls glass dissolution ($N = 2$). This is the case until β'_t reaches a value of about 0.2 g/g-fly ash at a reaction progress of $\alpha_t \approx 0.45$. The beginning of the relatively steep increase of β'_t at $\alpha_t \approx 0.45$ coincides with the change of the slope in Fig. 7a and b, and a change of the reaction grade to $N > 2$. Zeolite crystallization begins at $\alpha_t \approx 0.45$. It appears that the formation of a crust of zeolite on top of the gel layer (Fig. 4) affects the kinetics but does not shut down glass dissolution.

Crystallization of zeolite (Fig. 3) has a large impact on the mass δ_t (Eq. 4). There is a linear increase in the relative mass of fly ash actually dissolved up to $\alpha_t \approx 0.45$, followed by an apparent linear decrease to almost zero (Fig. 7b), though in reality α_t is increasing. The onset of the decrease is caused by zeolite precipitation. δ_t increases abruptly at $\alpha_t \approx 0.45$ because species not coming directly or not at all from the glass are imported into the surface layer.

K_N values (Eq. 9) were calculated for all fly ashes at 50 °C. Glass dissolution (K_1) was rate controlling for less than 10 h, except for CHP (72 h). K_1 characterizes the chemical durability of the glass and varies inversely with its content of network formers.

K_1 depends on temperature with an activation energy of 102 kJ/mol for HW and BSI, which is slightly higher than the values reported by Strachan [41] for nuclear waste glasses (70–90 kJ/mol) but is in good agreement with the value of 100 kJ/mol reported by Barkatt et al. [42]. K_N values were also calculated for the diffusion process. K_2 has lower activation energy than glass network dissolution. The values are 66 and 60 kJ/mol for HW and BSI fly ash, respectively. These values fall in the range of 41.8–83.7 kJ/mol measured for various glasses [43]. K_2 increases with increasing OH^- molarity at 75 °C (HW). Obviously, more OH^- is transported through the gel layer to the glass surface if more OH^- is available in solution. The dependence of K_2 on the OH^- molarity suggests that OH^- is the species limiting the rate at which the remaining glass reacts. An increase in the molarity of KOH by a factor of 10 increases K_2 by a factor of 3.

At W/S = 40, the glass phases of six fly ashes reacted almost completely within 2 weeks, except at 20 °C. Because of the high water content, the mixture remains slurry. The general reaction pattern is dissolution, gel formation, and zeolite precipitation as soon as the concentrations of SiO_2 and Al_2O_3 reach 0.1 and 0.05 M, respectively. This is the case at $\alpha_t \approx 0.45$. The molar Al/Si ratio in Linde F zeolite is 1. Condensation of Si and Al species precedes zeolite formation, i.e., formation of enough Si–Al oligomers with a ratio of Al/Si ≈ 1 is necessary. Condensation processes in alkaline solutions depend on the Al/Si molar ratio [39, 40]. Murayama et al. [44] reported that Si and Al species formed aluminosilicate gel followed by zeolite crystallization at high W/S.

Formation of a solid geopolymer typically occurs at lower W/S ratios such as 0.2–0.4. Decreasing the W/S ratio does not change the chemistry of the system dramatically, if the other variables are kept constant. Results to be reported in detail in a subsequent article show that glass dissolution is relatively small at W/S ≈ 0.35 as reaction

progress is limited due to shortage of water. Chemical attack of the glass network is better described by alteration of the structure and composition of the glass, i.e., direct conversion of glass into gel, rather than dissolution, particularly at higher reaction progress during hardening. For example, at $W/S \approx 0.35$, the amount of gel formed at a reaction progress of $\alpha_t = 0.2$ (75°C , 7.5 M KOH) is the same as that at $W/S = 40$ at $\alpha_t = 0.6$ with $\beta'_t \approx 0.4 \text{ g/g-fly ash}$. The onset of massive gel production at $W/S \approx 0.35$ starts at $\alpha_t < 0.1$, whereas for $W/S = 40$, not before $\alpha_t \geq 0.45$. At $\alpha_t < 0.3$ ($W/S \approx 0.35$), the geopolymers solid has practically no mechanical strength. At $\alpha_t \approx 0.35$, the reaction grade changes from $N = 2$ to $N > 2$. Further increase of α_t is small but is accompanied by a large increase in compressive strength.

Conclusions

We have developed a wet chemical method, which provides for a characterization of the kinetics of the reactivity of fly ash. We used the modified Jander equation to model the data. Three consecutive processes control reaction progress at $W/S = 40$: (1) A first order dissolution reaction which was accompanied by formation of a thin non-protective gel layer ($\alpha < 0.1$), (2) Transport (diffusion) through a thicker surface layer (mainly a gel of oxides of Fe, Ca, Mg, and Ti; $0.1 < \alpha < 0.45$), (3) Diffusive transport through a crust of zeolite, which formed on top of the gel layer ($\alpha > 0.45$). Rate constants were calculated for each process. The rate constant of the first process increased linearly with increasing concentration of network formers in the glass phase reflecting an intrinsic glass property: chemical durability. The rate constant of the second process increased with increasing OH^- concentration suggesting that OH^- may be the rate-limiting species.

Acknowledgements The authors are grateful for financial support of this project from the Vitreous State Laboratory (VSL) of The Catholic University of America (CUA). Chen Chen thanks the Chinese Overseas Fellowship Commission for financial support of his visit to VSL/CUA. The authors thank Dr. Hong Zhao, Dr. Andrew Buechele, and Dr. David McKeown (all VSL) for discussions and experimental support of this study. The authors are grateful to Dr. A. Barkatt (Department of Chemistry, CUA) for his comments and suggestions.

References

- Pacheco-Torgal F, Castro-Gomes J, Jalali S (2008) Constr Build Mater 22:1305
- Komnitsas K, Zaharaki D (2007) Miner Eng 20:1261
- Duxson P, Fernández-Jiménez A, Provis JL (2007) J Mater Science 42:2917. doi:[10.1007/s10853-006-0637-z](https://doi.org/10.1007/s10853-006-0637-z)
- Khale D, Chaudhary R (2007) J Mater Science 42:729. doi:[10.1007/s10853-006-0401-4](https://doi.org/10.1007/s10853-006-0401-4)
- Pacheco-Torgal F, Castro-Gomes J, Jalali S (2008) Mater 22:1315
- Fernández-Jiménez A, Palomo A (2005) Cem Concr Res 35:1984
- Fernández-Jiménez A, De la Torre AG, Palomo A, López-Olmo G, Alonso M, Armando MAG (2006) Fuel 85:1960
- Criado M, Fernández-Jiménez A, De la Torre AG, Aranda MAG, Palomo A (2007) Cem Concr Res 37:671
- van Jaarsveld JGS, Deventer JSJ, Lukey GC (2003) Mater Lett 57:1272
- Fernández-Jiménez A, Palomo A (2003) Fuel 82:2259
- Fernández-Jiménez A, Palomo A, Sobrados I, Sans J (2006) Micropor Mesopor Mater 91:111
- Palomo A, Alonso MM, Fernández-Jiménez A (2004) J Am Ceram Soc 87:1141
- Bumrongjaroen W, Muller I, Schweitzer J, Livingston RA (2007) In: Proceedings of the 2007 world of coal ash (WOCA), Covington, 2007
- Payá J, Borrachero M, Monzó VJ, Peris-Mora E, Amahjour F (2001) Cem Concr Res 31:41
- Shi CJ, Day RL (2000) Cem Concr Res 30:607
- Shi CJ, Day RL (2000) Cem Concr Res 30:51
- Biernacki JJ, Williams PJ, Stutzman PE (2001) ACI Mater J 98:340
- Antiohos S, Tsimas S (2004) Cem Concr Res 34:769
- Phair JW, van Deventer JSJ (2001) Mineral Eng 14:289
- Pietersen HS, Fraay A, Bijen JM (1990) Mat Res Soc Proc Symp 176:139
- Xu H, van Deventer JSJ (2002) Mineral Eng 15:1131
- Lee WK, van Deventer JSJ (2002) Colloid Surface A 211:49
- Buchwald A, Kaps Ch, Hohmann M (2003) In: Proceedings of the 11th international congress on the chemistry of cement (ICCC) Durban, 2003, p 1238
- Panagiotopoulou Ch, Kontori E, Perraki Th, Kakali G (2007) J Mater Sci 42:2967. doi:[10.1007/s10853-006-0531-8](https://doi.org/10.1007/s10853-006-0531-8)
- Mikuni A, Komatsu R, Ikeda K (2007) J Mater Sci 42:2953. doi:[10.1007/s10853-006-0530-9](https://doi.org/10.1007/s10853-006-0530-9)
- Fernández-Jiménez A, De la Torre AG, Palomo A, López-Olmo G, Alonso M, Armando MAG (2006) Fuel 85:625
- Sherman JD (1977) ACS Symp Ser 40:30
- Khawam A, Flanagan DR (2006) J Phys Chem B 110:17315
- Jander G (1927) Zeitschrift Anorg Allgem Chem 163:1
- Kondo R, Lee K, Diamon M (1976) J Ceram Soc (Japan) 84:573
- Dabic P, Krstulovic R, Rusic D (2000) Cem Concr Res 30:1017
- Krstulovic R, Dabic P (2000) Cem Concr Res 30:693
- Cabrera J, Rojas MF (2001) Cem Concr Res 31:177
- Grambow B (1985) Mat Res Soc Symp Proc 44:15
- Swaddle TW (2001) Coordin Chem Rev 219–221:665
- North MR, Swaddle TW (2000) Inorg Chem 39:2661
- Provis JL, Duxon P, van Deventer JSJ, Lukey GC (2005) Chem Eng Res Des 83:853
- Provis JL, van Deventer JSJ (2007) Chem Eng Sci 62:2309
- Weng L, Sagoe-Crentsil K (2007) J Mater Sci 42:2997. doi:[10.1007/s10853-006-0820-2](https://doi.org/10.1007/s10853-006-0820-2)
- Sagoe-Crentsil K, Weng L (2007) J Mater Sci 42:3007. doi:[10.1007/s10853-006-0818-9](https://doi.org/10.1007/s10853-006-0818-9)
- Strachan DM (2001) J Nucl Mater 298:69
- Barkatt AA, Gibson BC, Macedo PB, Montrose C, Sousanpour CJW, Boroomand MA, Rogers V, Penafiel M (1986) Nucl Technol 73:140
- Lasaga AC (1981) In: Lasaga AC, Kirkpatrick RJ (eds) Kinetics of geochemical processes. Mineralogical Society of America, Washington
- Murayama N, Yamamoto H, Shibata J (2002) Int J Miner Process 64:1